Augmenting the Performance of Acrylonitrile–Butadiene–Styrene Plastics for Low-Noise Dynamic Applications

Anirban Ganguly,[1] Swatilekha Saha,[2] Anil K. Bhowmick,[1] Santanu Chattopadhyay[1]

[1]*Rubber Technology Center, Indian Institute of Technology (IIT), Kharagpur 721302, India*
[2]*Department of Physics and Meteorology, Indian Institute of Technology (IIT), Kharagpur 721302, India*

Received 25 August 2007; accepted 19 January 2008
DOI 10.1002/app.28057
Published online 18 April 2008 in Wiley InterScience (www.interscience.wiley.com).

ABSTRACT: The main objective of this study was to enhance the performance of acrylonitrile–butadiene–styrene (ABS) plastics for dynamic structural applications, including those of automobile relevance. First, ABS was modified by blending with maleic anhydride grafted styrene–ethylene–butadiene–styrene block copolymer (MA-*g*-SEBS) in various proportions. Squeaking noise characteristics were evaluated by measurement of the frictional behavior in an in-house fabricated friction testing apparatus, and the results are explained on the basis of the change in surface energy upon modification. Detailed dynamic mechanical analyses (strain, frequency, and temperature sweep) revealed significant improvements in the damping characteristics of the modified ABS, especially that modified with 10 wt % MA-*g*-SEBS, without much sacrifice in its mechanical strength. The modulus values predicted with Kerner's model of the blends were well correlated with the morphological changes upon modification. © 2008 Wiley Periodicals, Inc. J Appl Polym Sci 109: 1467–1475, 2008

Key words: modification; structure–property relations; microstructure

INTRODUCTION

The use of plastics in automobiles has increased the flexibility of designers to use a variety of plastics of different sizes and textures in components. In most designs, the adjoining components are assembled in such a way that they remain in static contact, forming several interfaces. However, the motion of the automobiles causes the adjoining interfaces to be in relative motion with respect to each other. When the velocity of the automobile is low, this interfacial relative motion is accommodated by the deflection of the components, but as the automobile accelerates, the interfacial tangential force that deflects the components also increases. If the tangential force at the interface exceeds the static friction of the interfacial surface, the motion is no longer smooth, and it is basically a combination of component deflection and sliding (which accommodates the force imbalance). When sliding starts, the tangential frictional force decreases (because the coefficient of static friction is greater than the coefficient of kinetic friction). This imbalance of force, which initiates the stick–slip motion[1] and causes noise, for example, squeaks (produced due to the elastic deformation of the contact surface), is highly disturbing to the passenger.[2] When impulsive force (high magnitude of force acting for a short interval of time) acts on automobile parts, it causes the relative motion of components with a brief loss of contact. Loosely assembled automotive parts (or when there is a gap between the automobile components or if they are very flexible), when subjected to such force, rattle. Thus, in rattling,[1] impacts are caused when the adjacent surfaces move perpendicular to each other with repeated contact and a loss of contact due to the improper assembling of components. An audible rattle lies at a comparatively low frequency range. Higher frequency range rattles are known as *buzzes*.[3] Squeaks and rattles are now increasingly perceived as indicators of how the automobile was built. Hence, the need to reduce these noises is a major concern for the manufacturers.

Because of suspension inputs, the stick–slip cycle occurs at a relatively lower frequency range, but the energy released produces a vibration in the audible range. The material constituents, coefficient of friction, normal load, and load history and various other factors determine the amplitudes and frequencies of the squeaks and rattles.[3] Structural deficiencies, incompatible material pairs, or poor geometric controls are almost always the cause of squeaks and rattles.

Earlier studies in this area concentrated on better design principles. However, these can only reduce the noises to some extent because the functionality

Correspondence to: S. Chattopadhyay (santanuchat71@yahoo.com).

of the subsystem of the automobile, for example, the sliding of the seats and various operations of doors and windows, demand movement. In addition to this, changes in physical parameters such as temperature and humidity conditions cause dimensional variations in components (e.g., expansion on heating) that are more prominent, especially in plastics.[3] Hence, it is apparent that material pair interaction cannot be avoided. Thus, as the relative motion cannot be eliminated, material pair compatibility is highly desirable. Previously, slip coatings,[4,5] antisqueak molding,[6] and surface finish textures on elastomeric and thermoplastic contact locations had been tried by manufactures, but this yielded unsatisfactory results, perhaps due to the wear and variation of the physical parameters over time. Different material pairs that increase the surface friction have also been studied.[7] The effect of sliding velocity, normal load, surface roughness, and environmental factors on materials has also been studied widely for noise reduction.[8] Various techniques have been adopted for arresting the squeaking and rattling noises.[4–6,9–13]

In this study, we worked with acrylonitrile–butadiene–styrene (ABS) plastics, which are frequently used in the interiors of automobiles,[14] such as in front panels, fenders, seat backing, and roof covers, because of its excellent mechanical properties (e.g., very high strength and overall toughness) and very good surface finish. A comprehensive correlation of squeak and rattle noises with respect to the surface friction and the internal friction (damping) of the materials has not yet been reported in detail. Modification of the microstructure of the components of ABS were attempted to reduce the acoustic noises.

Maleic anhydride grafted ($\sim$ 2% grafting) styrene–ethylene–butylene–styrene block copolymer (MA-*g*-SEBS) was chosen to be blended with ABS because both have styrene in their respective structures, and the maleic anhydride group should have increased the compatibility of the blend by polar–polar interaction. The blend was expected to improve the frictional characteristics of the surface. We speculated that the polar groups present in the blend would rise to the surface, and therefore, we expected a resultant rise in the surface friction. These, in turn, were expected to reduce the squeaking events. As the internal damping characteristics increased on the incorporation of MA-*g*-SEBS in ABS, the lower frequency rattle noise would be automatically dealt with. Because the automotive interiors demand excellent mechanical properties, the percentage MA-*g*-SEBS used in the modification of ABS was kept low (5, 7, 10, and 15%, respectively) so that the drop in the modulus and failure properties of ABS remained within the tolerance limit.

The objective of our study was to tailor the ABS blends in such a way to improve the surface friction (to minimize squeak) and damping (to reduce rattle) without compromising much of the mechanical properties.

EXPERIMENTAL

Materials

MA-*g*-SEBS (Kraton FG 1901 X) was procured from Shell Chemical Co. (Belpre, OH; presently marketed by Kraton, Ltd.); it had 1.8% maleic anhydride grafted to the styrene–ethylene–butylene–styrene (SEBS) backbone. ABS (extrudable grade, Cycolac X15) (Texas, USA) was procured from G. E. International. Cyclohexane and formamide were analytical grade and were purchased from Aldrich (Mumbai, India).

Blending and molding

The melt blending of ABS and MA-*g*-SEBS in 5, 7, 10, and 15 wt %, respectively was carried out in a sigma mixer (S. C. Dey & Co., Kolkata, India) at 200°C for 4 min at a 40-rpm rotor speed. The samples were compression-molded at a temperature of 210°C with a preheating time of 1 min and at a pressure of 5 MPa in a George. E. Moore & Son, Ltd. (Birmingham, United Kingdom) compression-molding machine.

Friction measurement

The friction test was carried out on a Zwick (model 1445) universal testing machine (Ulm, Germany). The in-house fabricated apparatus setup is shown in Figure 1. The tests were carried out on an aluminum friction table at 25°C with sliding speeds of 10 and 100 mm/min, respectively. With a Talysurf surface roughness measuring machine (TN, USA), the roughness of the table surface was found to be 0.72 μm, and the normal force applied was 0.05 kg. All of the results reported here are the averages of three readings.

Contact angle and surface energy measurements

The sessile drop method was adopted for contact angle measurement with water and formamide as the probe liquids in a Kernco (model G-II) (Texas, USA) contact angle meter. The polymer plate used in the experiment had dimensions of 10 $\times$ 10 $\times$ 0.5 mm with an almost similar surface roughness ($\sim$ 1 nm). Each value reported had a maximum error in the contact angle of the liquid with the solid surface (θ) of $\pm$ 0.2, and the mean of at least five readings was taken. Fowkes[15] proposed that the surface energy of a solid (γ_s) is the sum of the contributions

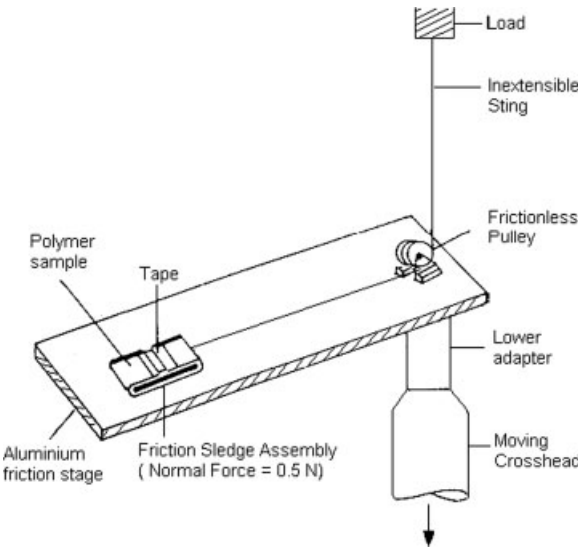

Figure 1 Schematic setup of the frictional measurements.

from the polar component (γ_s^p) and dispersive component (γ_s^d) of the surface energy as follows:

$$\gamma_s = \gamma_s^d + \gamma_s^p \tag{1}$$

For a solid–liquid system, different components of the surface energy can be calculated from the following equation:[16,17]

$$\cos\theta = \frac{2\sqrt{(\gamma_s{}^d\gamma_l{}^d)}}{\gamma_l} + \frac{2\sqrt{(\gamma_s{}^p\gamma_l{}^p)}}{\gamma_l} - 1 \tag{2}$$

with negligible spreading pressure assumed. The subscripts s and l represent the solid and liquid phases, respectively, and the superscripts d and p represent the dispersive and polar components, respectively, of the surface energy.

With the previous equations and the following values[18] of γ_l^d and γ_l^p of the probe liquids, γ_s^p was calculated (water: γ_l = 72.8 mJ/m^2, γ_l^d = 21.8 mJ/m^2, γ_l^p = 51.0 mJ/m^2; formamide: γ_l = 58.2 mJ/m^2, γ_l^d = 39.5 mJ/m^2, γ_l^p = 18.7 mJ/m^2).

Dynamic mechanical thermal analysis (DMTA)

The DMTA measurements were carried out in a DMTA-IV instrument (Rheometric Scientific, Inc., NJ, USA). Temperature scans were performed between −50 and 150°C at a frequency of 1 Hz and a strain of 0.05%. Frequency and strain sweep measurements for all of the samples were performed at room temperature and 70°C, respectively. Frequency was varied from 0.03 to 20 Hz for the frequency sweep at constant strains of 0.01 and 0.1%, respectively. Strain sweep was performed at a specified frequency of 0.5 Hz. The data were analyzed with RSI Orchestrator (NJ, USA) application software.

Scanning electron microscopy (SEM)

The SEM photomicrographs of the blends were taken with a JSM 5800 microscope (Jeol, Tokyo, Japan) with an accelerating voltage of 15 kV. The SEBS portions in the blends were etched out with cyclohexane, and the samples were dried. To investigate the bulk, thick portions were taken, cryofractured, and etched subsequently before the scan. Sputter coating with gold was done before the SEM studies.

Mechanical properties

The studies of the mechanical properties were carried out in a Hioks-Hounsfield universal testing machine (Test Equipment, Ltd., Surrey, England). The tensile specimen was punched with ASTM Die-C. The tests were carried out as per ASTM D 412-98. The stress–strain curve was plotted with Lab Tensile software (Surrey, England), from which the tensile strength and percentage elongation were calculated. The tensile properties reported here were calculated on the basis of the average results of five findings.

RESULTS AND DISCUSSION

Frictional properties

The dependence of static friction with increasing percentage of MA-*g*-SEBS on two contact surfaces, namely, aluminum (Al) and ABS, is shown in Table I. The introduction of rubbery MA-*g*-SEBS increased the frictional force with a sliding velocity of 10 mm/min, as shown in the traces in Figure 2. It was evident from the trace that the amplitude and frequency of the stick–slip events significantly declined with the incorporation of MA-*g*-SEBS (10 wt %). This implied that the noises created by stick–slip events would obviously be subdued upon rubber modification. This trend remained indifferent with changes in the sliding surface (Al and pure ABS) and sliding velocity (10 and 100 mm/min, not shown). The influence of MA-*g*-SEBS on the static friction with an Al contact surface is depicted in Figure 3. The frictional force of ABS exhibited an increase with increasing percentage of MA-*g*-SEBS in the blends. The reason for this increase was the incorporation of a relatively soft rubbery phase. The modulus of the modified surface decreased (as illustrated in later sections), and their effective contacts with the sliding surfaces increased. This is evident, as shown in Table I, where 100% MA-*g*-SEBS registered the highest frictional force with both surfaces, ABS and Al. In addition, the change in the surface energy of ABS upon modification contributed to the overall change in the surface friction. This is depicted in corroboration with the surface energy measurement in following section. We also observed that up to 10% MA-*g*-

TABLE I
Variation of γ^p and Static Friction with the Percentage of MA-*g*-SEBS

MA-*g*-SEBS (wt %)	Static frictional force (mN) with an Al metal contact surface	Static frictional force (mN) with an ABS contact surface	γ_s^p (mJ/m^2)
0	437 ± 3	484 ± 3	8.5
5	491 ± 2	500 ± 4	14.5
7	500 ± 2	628 ± 6	17.0
10	529 ± 3	657 ± 4	21.3
15	508 ± 4	624 ± 5	22.9
100	1421 ± 4	1500 ± 8	30.5

SEBS content, the surface friction increased steadily, beyond which there was a slight decrease in its values. This may have been due to the fact that a further increase in the percentage of MA-*g*-SEBS proceeded toward bulk modification. This phenomenon is discussed further in the ensuing sections.

The dependence of γ^p on the percentage of MA-*g*-SEBS is revealed in Table I. It is clear from the data that γ^p increased with increasing MA-*g*-SEBS. The polar groups (e.g., the maleic anhydride, the nitrile groups) rose to the surface and increased the polarity of the surface (and increased γ^p). Examining Table I further, we observed that the increase in surface friction with the ABS contact surface was higher than that with metal contact surface. This occurrence may be attributed to the higher ABS–modified ABS polar–polar interaction compared to the ABS–metal interaction.

Frictional force, as mentioned in an earlier context, played a significant role in the determination of the extent of stick–slip events that occurred between the contact surfaces when they produced relative motion. This stick–slip phenomenon was markedly reduced if the frictional force exceeded a critical value. The magnitude of the frictional force achieved for the modified ABS containing even as low as 5% MA-*g*-SEBS was much higher than those reported by Akira et al.[13] with a antisqueak poly(tetrafluoro ethyelene) [PTFE] system. Thus, the frictional forces achieved in our modified systems should have been sufficient enough to prevent the squeak events in this approach of the introduction of a small amount of MA-*g*-SEBS into the ABS matrix.

DMTA

DMTA is one of the most important techniques used to reveal the viscoelastic properties, internal friction, and molecular level interactions of polymer blends. Thus, DMTA is an essential tool for appraising the morphology of polymer blends. Sound and vibration damping characteristics of polymers, polymeric blends, composites, or laminates are evaluated with the help of dynamic mechanical analysis.[9]

Figure 4 displays the plot of tan δ versus the frequency of the 10% MA-*g*-SEBS blend at two different

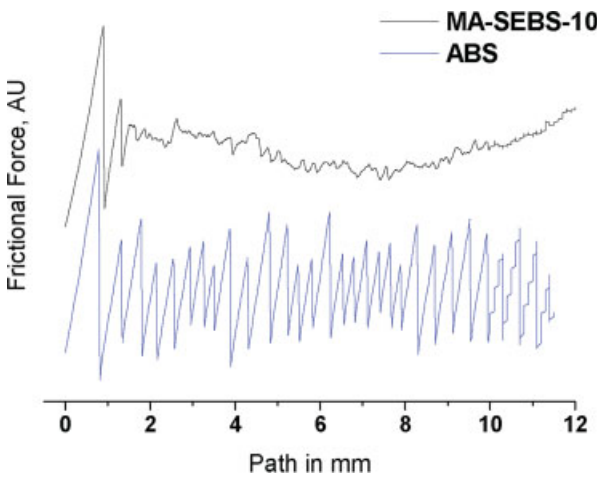

Figure 2 Traces of the frictional measurements on the aluminum surface of ABS and ABS with 10% MA-*g*-SEBS with a sliding speed of 10 mm/min. [Color figure can be viewed in the online issue, which is available at www.interscience.wiley.com.]

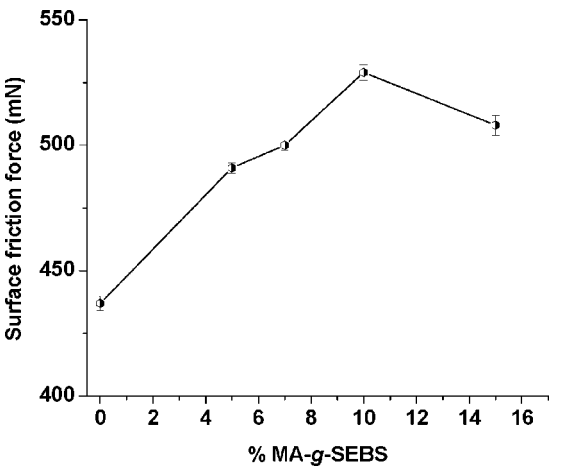

Figure 3 Change in the static friction of ABS with an Al metal contact surface as a function of the percentage of MA-*g*-SEBS.

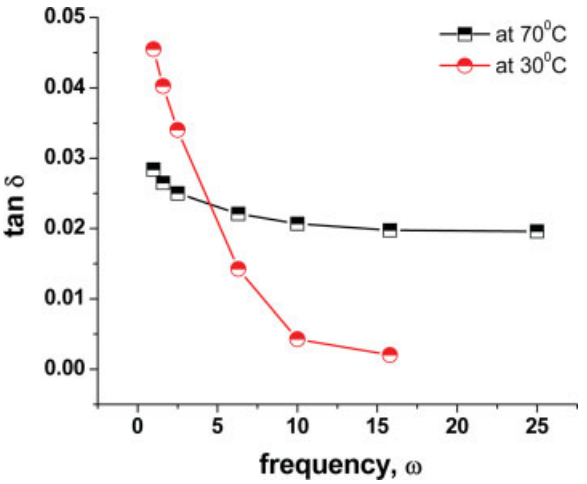

Figure 4 Tan δ versus frequency (Hz) at 70 and 30°C for the 10% MA-*g*-SEBS blend. [Color figure can be viewed in the online issue, which is available at www.interscience.wiley.com.]

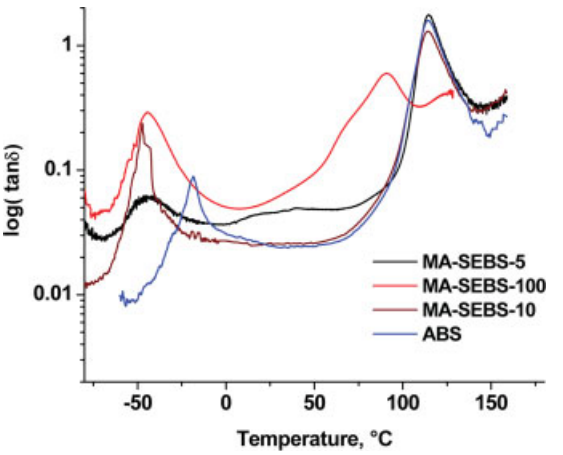

Figure 6 Variation of the damping factor with temperature at 0.01% strain and at a frequency of 1 Hz. [Color figure can be viewed in the online issue, which is available at www.interscience.wiley.com.]

temperatures (70 and 30°C). From the plot, one can observe that the damping factor was higher in the lower frequency range at 30°C, that is, approximately at room temperature. This indicates that the 10% MA-*g*-SEBS blend could definitely reduce rattling. Also, we analyzed the tan δ versus frequency of 10% MA-*g*-SEBS at high temperatures (from the time–temperature superposition principle, it corresponded to that at low frequency), to further emphasize the former statement. Obviously, the blends containing 5% MA-*g*-SEBS would be even better dampers (for both rattling and buzzing) for noise because it registered a higher tan δ at wide ranges of temperatures (shown later with Fig. 6), which essentially corresponded to a wide range of frequency following the time–temperature correspondence principle as stated previously. Figure 5 shows the plot of log (tan δ) versus log ω at 24°C and 0.01% strain. The tan frequency of oscillation (δ) corresponding to 10% MA-*g*-SEBS blend was between the two controlled states (i.e., pure ABS and MA-*g*-SEBS). Thus, this proves that blending the ABS matrix with MA-*g*-SEBS indeed increased the damping factor.

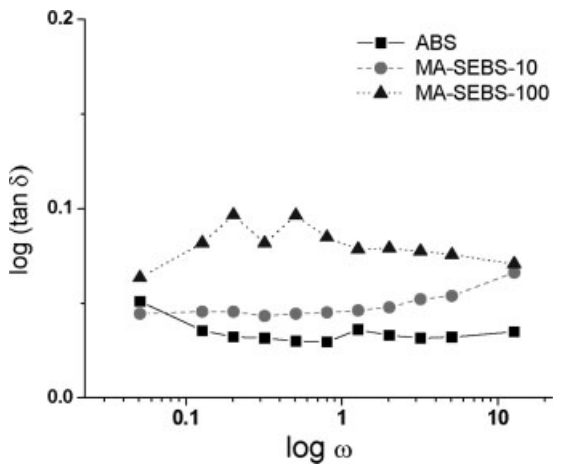

Figure 5 Variation of the damping factor with frequency at 0.01% strain and 24°C.

The plot of tan δ versus temperature (°C) for the blends is revealed in Figure 6. With increasing MA-*g*-SEBS content in the ABS matrix, the low-temperature relaxation peak of ABS shifted toward the glass-transition temperature of the ethylene–butylene part of MA-*g*-SEBS. It is interesting to note that in all of the blends, the peak corresponding to the relaxation of the styrenic portion of the block copolymer disappeared. The blends registered a high-temperature relaxation peak corresponding to the styrene–acrylonitrile part of ABS.[14] For the blends containing 5% MA-*g*-SEBS, broad relaxation spectra covering a wide range of temperatures (0–100°C) along with relaxation peaks at lower and higher temperatures (corresponding to the ethylene–butylene portion of MA-*g*-SEBS and the styrene–acrylonitrile portion of ABS, respectively) were observed. These can only be explained by the molecular level association of MA-*g*-SEBS with the ABS polymer. The change in the relaxation behavior for the blends containing 10% MA-*g*-SEBS, for obvious reasons, portended the beginning of phase separation. The shift was, however, more distinct for 15% MA-*g*-SEBS (not shown).

In Figure 7, the storage modulus from frequency sweep at 25°C is shown. The value of the storage modulus for the 5%MA-*g*-SEBS blend exceeded that of pure ABS. This may be explained by synergistic

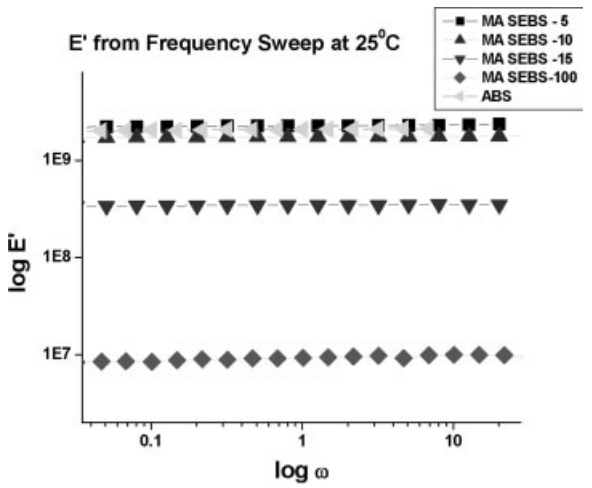

Figure 7 Storage modulus from frequency sweep at 25°C.

reinforcement by 5% MA-*g*-SEBS, mostly because of molecular-level miscibility in the ABS (which was polar) matrix, which led to an increase in the low-strain dynamic modulus. The storage modulus of the 15% MA-*g*-SEBS blend decreased by almost 10 times, which signified the onset of phase separation, which was expected due to the high percentage of the MA-*g*-SEBS contribution. We also noted from the frequency sweep of neat MA-*g*-SEBS that the same expected storage modulus (E') value of 10 MPa (at 25°C) was obtained.

The variation in storage modulus with strain of selected blends is shown in Figure 8. The storage modulus of blends containing 5% MA-*g*-SEBS was higher than that of the pristine ABS. However, the storage modulus decreased with further increases in MA-*g*-SEBS content of the blend. This occurrence can be explained in same manner as described earlier. A drastic reduction in the storage modulus at higher strain amplitude for the blends containing 10% MA-*g*-SEBS can again be attributed to the change in morphology (onset of phase separation), which is elaborated in the following sections.

Thus, from the previous discussion, we conclude that blending the ABS matrix with MA-*g*-SEBS initially, with small percentages, strengthened the ABS matrix by mixing in the molecular level. Further increasing the percentage MA-*g*-SEBS initiated phase separation, which was further justified by the Kerner model and SEM morphological analysis, as discussed in the following section.

Kerner model

We predicted the storage modulus of the ABS blend with Kerner's foam model.[20] We assumed that the morphology was a dispersion of MA-*g*-SEBS in spherical form on the ABS matrix (we neglected the MA-*g*-SEBS modulus because the percentage of MA-*g*-SEBS in the blend was too small to cause any significant change in the modulus, and most importantly, the dynamic modulus of pristine MA-*g*-SEBS was approximately two and half orders less than that of ABS). The modulus of the blend (E_{blend}) in the foam model is then given by

$$E_{\text{blend}} = E_{\text{ABS}} \Big/ \left[1 + \frac{15 \times (1-\nu)}{(7-5\nu)} \times \left(\frac{\phi_{\text{SEBS}}}{\phi_{\text{ABS}}}\right)\right] \quad (3)$$

where E_{ABS} is the modulus of ABS, ν is the Poisson ratio (0.3 corresponds to absolute plastic and 0.5 corresponds to absolute elastomer), and ϕ_{SEBS} and ϕ_{ABS} are the volume fractions of MA-*g*-SEBS and ABS, respectively, in the blends. When the modulus was calculated with eq. (3), we found that for lower percentages of MA-*g*-SEBS (5 and 7%), the experimental value of the storage modulus exceeded the predicted value, and the correspondence between the calculated and experimental results was best for lower values of the Poisson ratio. This result reinforced our previous argument that at lower percentages of MA-*g*-SEBS, molecular level miscibility was predominant, which increased the intermolecular interactions. Furthermore, with increasing amount MA-*g*-SEBS (10 and 15 wt % MA-*g*-SEBS blends), the theoretical value for storage modulus was more than that of the experimental ones. The correspondence between the theoretical and experimental results was best near $\nu = 0.45$, which again justified our previous finding that at higher percentages of MA-*g*-SEBS, phase separation began. The best fit was found at 10 wt % MA-*g*-SEBS with $\nu = 0.42$ (for both frequency and strain sweep). However, for the blend containing 15 wt % MA-*g*-SEBS, the divergence between the predicted and experimental storage modulus values

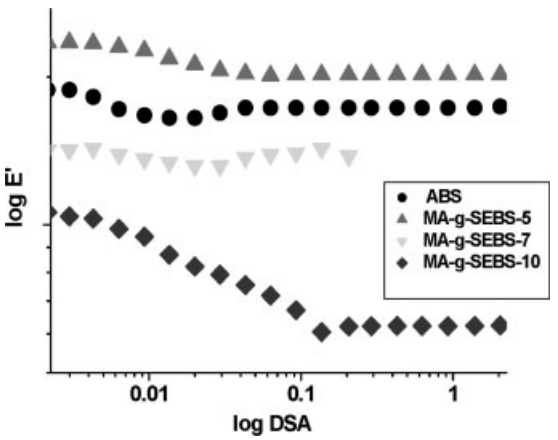

Figure 8 log–log plot of the storage modulus versus double strain amplitude (DSA) at 25°C.

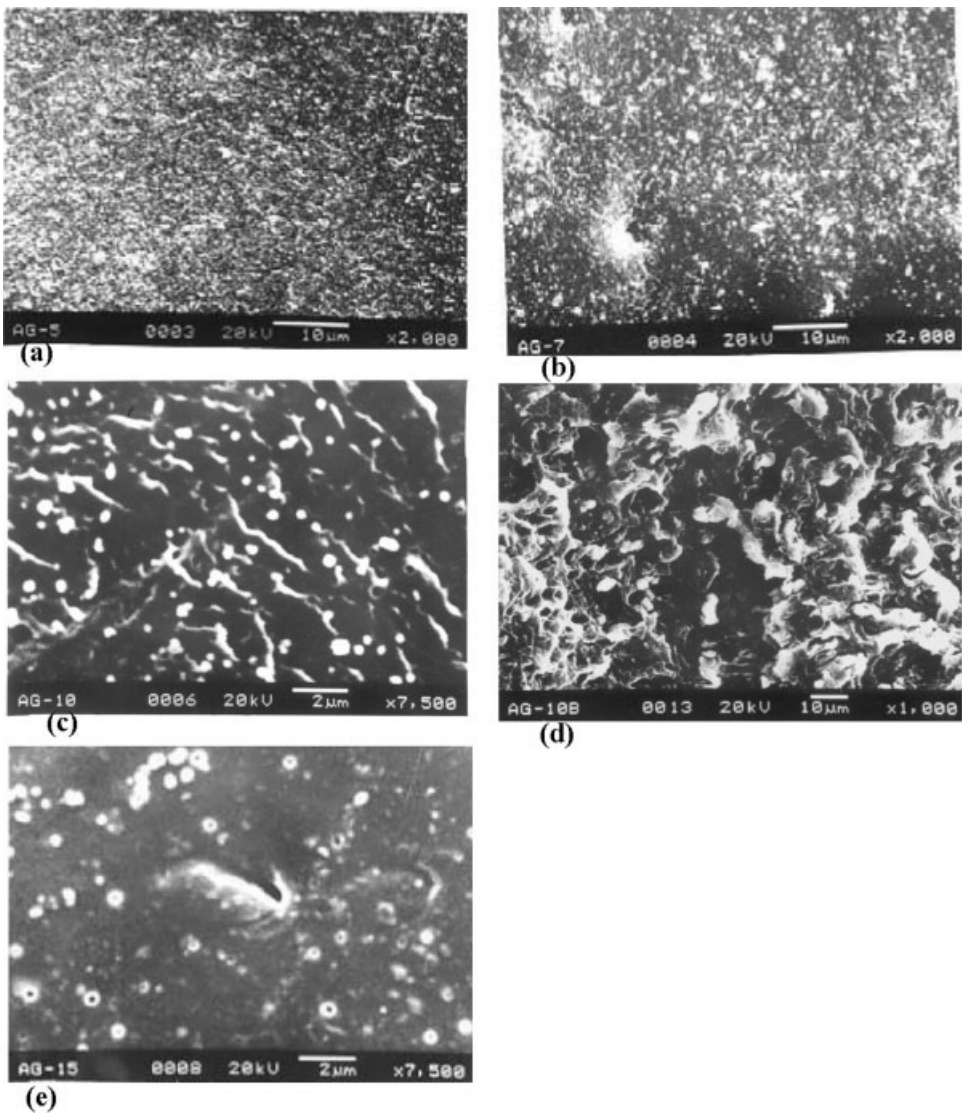

Figure 9 SEM photomicrograph of the (a) 5% MA-*g*-SEBS blend surface, (b) 7% MA-*g*-SEBS blend surface, (c) 10% MA-*g*-SEBS blend surface, (d) 10% MA-*g*-SEBS blend bulk, and (e) 15% MA-*g*-SEBS blend surface.

was even more notable and gave the best correspondence, even at higher values of the Poisson ratio. At this stage, it is imperative to state that the Kerner's foam model could account for a qualitative visualization of the microstructure of this system. However, to make it more quantitative, one has to implement the contribution from the MA-*g*-SEBS phase and their interface with the ABS matrix in the model. In that case, the sensitivity of the model toward the level of strain, intermolecular interaction, and frequency would be more pronounced. Work in this direction has been taken up by our group, a detail of which will be published in the future. However, Kerner's foam model as such was very good for a qualitative depiction of this system, as explained earlier.

Morphology as determined by SEM

Figure 9(a–e) shows the SEM photomicrographs of the ABS and MA-*g*-SEBS blends. The dark domains inside the white protrusions indicate the positions of the extracted MA-*g*-SEBS phase. ABS was found as the continuous matrix. Figure 9(a,b) shows MA-*g*-SEBS creating a cocontinuous phase on ABS for the blends containing 5 and 7% MA-*g*-SEBS. For 10% MA-*g*-SEBS, a partial commencement of phase separation at the surface is shown in Figure 9(c). The bulk image of the fractured sample [Fig. 9(d)] showed distinctly the phase separation at the bulk on the furrows of the fractured surface. Blends containing 15% MA-*g*-SEBS clearly indicated discrete spherical phase formation [Fig. 9(e)]. Thus, the morphological analyses with SEM reinforced our previ-

TABLE II
Mechanical Properties of the Samples at Room Temperature (31°C)

% SEBS (phr)	Tensile strength (MPa)	Stress at 5% (MPa)	Elongation at break (%)
0	25.9	23.69	14
5	19.0	18.05	13
7	18.7	17.40	14
10	19.0	14.80	19
15	17.2	14.75	26
100	17.3	1.75	820

ous analyses of the surface properties and dynamic properties.

Mechanical properties

In the previous sections, we examined in detail the effect of MA-*g*-SEBS on the ABS matrix. Because ABS offered excellent mechanical properties, we needed to study by what percentage the blending reduced the tensile strength, stress at 5%, and overall toughness, that is, if the reduction is at all within the tolerance limit for engineering automobile applications. Table II summarizes the dependence of tensile strength, stress at 5% extension, and elongation at break with increasing MA-*g*-SEBS. This indicates that an effective improvement in elongation at break for ABS with the incorporation of MA-*g*-SEBS started only after a 10% content of the latter phase was added (which coincides with our discussion). As shown in Table II, both the tensile strength and stress at 5% decreased with MA-*g*-SEBS content.

Tensile strength, being a failure property, depends much on the number of defects and stress sharing. At lower proportions of MA-*g*-SEBS, macroscopic defects were expected to be nonuniformly distributed in the ABS matrix. As the amount of SEBS was increased after a certain proportion, uniform microscopic phase separation provided a mechanism for load sharing.

Hence as a whole, we observed that blending MA-*g*-SEBS with ABS reduced the overall mechanical properties, but the percentage decrease was within the tolerance limit, at least up to 10 wt % incorporation of MA-*g*-SEBS. With the blend containing 10% MA SEBS, less than a 27% decrement of tensile strength compared to its original value was observed. Thus, we did not compromise much in terms of the mechanical properties, which is very essential for engineering plastics, especially for automotive interior applications.

CONCLUSIONS

In this analysis, we blended ABS with 5, 7, 10, and 15 wt % of MA-*g*-SEBS and observed that up to a 10% MA-*g*-SEBS proportion, the surface friction increased, which should reduce squeaking noises. The damping factor also increased significantly without much reduction in the storage modulus. This ought to decrease rattling. Hence, we conclude that the best window of composition is between 5 and 10%, in which one can achieve maximum surface modification and modified dynamic properties even without a significant sacrifice in the mechanical properties.

Further increases in the MA-*g*-SEBS content modified the bulk properties, which is not desirable, as it may tamper with structural applications, particularly in the interior parts of automobiles. The morphological changes of ABS on the incorporation of rubbery MA-*g*-SEBS in the blends gave rise to suitable surface and damping characteristics, as shown by the dynamic mechanical analysis over a range of temperatures.

Theoretical studies of the dynamic properties with Kerner's foam model predicted that 10% MA-*g*-SEBS gave the best fit for storage modulus, beyond which (e.g., 15% MA-*g*-SEBS) the experimental storage modulus diverged from the Kerner model prediction, which implied bulk modification with prominent phase separation. This was further consolidated from morphological studies by SEM photomicrographs.

The authors are grateful to Jinu Jacob for helping with the DMA measurements. Help from the SEM facilities, Central Research Facility (CRF), IIT Kharagpur, is also kindly acknowledged.

References

1. Polt, G.; Sebestyen, T.; Pauschitz, A.; Franek, F. Mater Sci Forum 2005, 473–474, 249.
2. Eiss, N. S.; Lee, E. In Book of Abstracts, 216th ACS National Meeting; American Chemical Society: Washington, DC, 2000; Chapter 26, p 418.
3. Kavarana, F.; Rediers, B. Sound Vibration 2001, 35 (April), 1 (Presented at SAE 1999 Noise & Vibration Conference & Exposition, Traverse City, MI, May 1999; paper #1999–01–1728 ©1999 SAE, Inc.).
4. Riestenpatt, H. (to Perdue). U.S. Pat. 6,624,229 (2003).
5. Agrawal, R. K.; Thomas, J. F. U.S. Pat. 5,255,483 (1993).
6. Gross, M. G.; Young, J. D. U.S. Pat. 5,338,087 (1994).
7. Eiss, N.; Lee, E.; Trapp, M. Proceedings of the Noise and Vibration Conference, Traverse City, MI May 1997; SAE paper 972056; p 1479.
8. Martin, T.; Roman, P. SAE Trans 2003, 112, 1818.
9. Corsaro, R. D.; Sperling, L. H. ACS Symposium Series 424; American Chemical Society: Washington, DC, Sound and Vibration Damping with Polymers. 1990.

10. Kato, S.; Murase, M. Jpn Kokai Tokkyo Koho JP 2002309176 A (2002).
11. Matsutani, K.; Ichikawa, S. Jpn Kokai Tokkyo Koho JP 08281210 (1996).
12. Okamura, Y.; Yasugi, M.; Yoshinaka, T. Jpn Kokai Tokkyo Koho JP 54139610 (1979).
13. Yanagi, A.; Yamamoto, S.; Osanaga, T.; Sakai, S.; Michigami, Y.; Matsuoka, S; Akira. Jpn Kokai Tokkyo Koho JP 2000026787 (2000).
14. Motschall, E.; Anwendusgstech, A. Farbenfabriken Kunstst-Plast (Solothurn, Switzerland) 1968, 15(2), 46.
15. Fowkes, F. M. In Treatise on Adhesion and Adhesives; Patrick, R. L., Ed.; Marcel Dekker: New York, 1967; Vol. 1.
16. Owens, D. K.; Wendt, R. C. J Appl Polym Sci 1969, 13, 1741.
17. Kaelbe, D. H.; Uy, K. C. J Adhes 1970, 2, 50.
18. Konar, J.; Sen, A. K.; Bhowmik, A. K. J Appl Polym Sci 1993, 48, 1579.
19. Mott, P. H.; Roland, C. M.; Corsaro, R. D. J Acoust Soc Am 2002, 111, 1782.
20. Kerner, E. H. Proc Phys Soc B 1956, 69, 808.